Role of impact on determination of interfacial toughness measurement by indentation for thermal barrier coating systems

B. Ekici*

The measurement of interfacial toughness by an indentation method was proposed several years ago. It has been shown that this method is very simple and reliable for the calculation of interfacial toughness. For this reason, many studies were performed for different substrate and coating combinations. Numerical models also supported these studies. Unfortunately, the success of this method depends on the hardness of the substrate. In most studies, the coating was ceramic and the substrate was steel. The substrate must be hard enough to get a circular crack around the indentation zone. If the substrate is not hard enough, the circular crack cannot be seen. In the light of the experiments performed for different combinations of substrate and coating, the use of the method was restricted to a very narrow range of materials that are mainly used for thermal barrier coating systems. In the present study, this method is used even for a medium hardness substrate. In order to get a circular crack, loading is performed with constant acceleration instead of static loading. The success of the method is shown to be considerably increased.

Keywords: Thermal barrier coatings, Impact, Interfacial toughness, Indentation

List of symbols

EBPVD	electron beam physical vapour deposition
G	energy release rate
D	damage parameter
K_c	interfacial fracture toughness
σ	stress
ε_r	radial strain
$\dot{\varepsilon}$	strain rate
ε_θ	circumferential strain
$\bar{\varepsilon}^p$	effective plastic strain
$\dot{\varepsilon}^*$	effective plastic strain rate
ε^f	fracture strain
V	Poisson's ratio
U	radial displacement
R	radial position
D	depth of indentation
A	projected indentation in radial direction
ΔT	change in temperature
ΔL	change in length
Δh	depth of indentation
V	velocity of indenter
α	thermal expansion coefficient

Introduction

Thermal barrier coating (TBC) systems are mainly used in gas turbine applications because they have many advantages such as combined corrosion and heat resistance. They are very important, especially for aircraft engines, which have critical components such as combustors, vanes and blades. These components must be insulated and protected against heat and corrosion, otherwise it would not be possible to produce an efficient jet engine. TBC systems can lead to an increase in engine efficiency by increasing the operating temperature of these components. However, the full use of TBC insulating capacity requires a high degree of confidence in the structural endurance of the coating. Loss of adhesion of TBCs to the substrates is a key barrier to their full exploitation. Interface toughness between coating and substrate has been the main focus of many studies.[1] To improve the interfacial toughness of TBC systems, graded coating methods have been employed in recent studies.[2] In addition to manufacturing improvements, ceramic and metal interfaces have also been studied on an atomic scale.[3] Ceramic and metal interfacial failure mechanisms determine the durability of TBC systems.[4]

Although many studies have been performed in this field to increase interfacial toughness, the first step is to find a reliable method to measure interfacial toughness to judge the success of TBC systems. This method must be simple and reliable. Vasinonta and Beuth[5] proposed an interfacial toughness measurement method, in which a simple indentation very similar to the Rockwell test was used. The interfacial fracture toughness is related to the strain energy release rate G. The value of G is correlated with the radius of the crack formed during indentation. Measurement of the crack radius is essential input data for calculating the interfacial

Department of Mechanical Engineering, Goztepe Kampusu, Kadikoy 81040, Istanbul, Turkey

*Corresponding author, email ekici@eng.marmara.edu.tr

Published by Maney on behalf of the Institute
Received 8 October 2004; accepted 26 May 2005
DOI 10.1179/174329405X68605

toughness energy. It is simple and reliable. Their indentation method has been repeated for hard elastic films on elastic–plastic soft substrates[6] and for strong films on a ductile substrate.[7] It was found that the parameters of the coating and the substrate both affect the formation of a circular crack around the indentation zone. The most important parameters are the coating thickness and the substrate material. The prestresses in the coating vary, depending on the TBC system. These prestresses affect the radius of the circular crack and therefore the interfacial toughness energy.[8]

Other studies focused on increasing the efficiency of this method by changing the indenter shape. Analysis of a wedge impression test for measuring the interface toughness between the films/coatings and ductile substrates was proposed by Begley *et al.*[9] Wedge type indenters were tried instead of a conical indenter, and some improvements were obtained.

Although measuring interfacial toughness by experiment has been successful by this simple indentation method for TBC systems, there are some restrictions. The first restriction is that the substrate must be hard enough, otherwise deformation in the substrate zone under the indenter nose is too great to create a visible circular crack. The second restriction is to calculate parametric effects such as coating layer, coating type and residual stress patterns etc. Finite element and boundary element modelling methods have been employed to find the effects of such methods on interfacial toughness calculations.[10]

The reason for the first restriction is that the velocity of deformation in the substrate in the indentation direction is very high with respect to the velocity of deformation in the coating in the radial direction. Toughness and damage behaviour of plasma sprayed ZrO_2 thermal barrier coatings have been studied to find the effect of velocity for a specific type of TBC system.[11] If the velocity of deformation in the substrate in the indentation direction and the velocity of deformation in the coating in the radial direction are close to each other, a circular crack radius can be obtained. In order to obtain this effect, impact loading needs to be applied instead of static loading.

In the simple indentation method, a specimen is placed in a Rockwell hardness tester using a Brale C indenter. The indenter penetrates the coating, and the plastic deformation of the underlying substrate material induces compressive radial stresses in the substrate, away from the indent crater.[12] The toughness can be determined from the measurement of the delaminating radius,[13] with assumed or measured values of the coating thickness, coating residual stresses and elastic properties of the coating and substrate materials.[14]

In the present study, the same indentation method is employed, but the loading is dynamic instead of static as used in the literature. This loading pattern is useful for any TBC system, whether or not the substrate is hard. A circular crack is obtained, and the interfacial fracture toughness is measurable for all types of TBC systems.

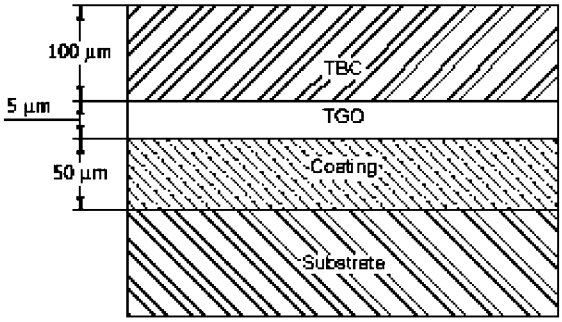

1 TBC system

Materials and methods

Model

In the present model, a large substrate with a refined mesh around the indentation zone and three coating layers is used. Studies of TBC systems have shown that an amorphous film at the interface between the coating and the substrate of thermal barrier coatings is produced by plasma spraying.[15] Therefore this amorphous layer must be considered in the model. A standard TBC specimen sized model can then be used to generate results specifically for application to TBC specimens, with indentation by a rigid indenter with a rounded tip identical to that of an actual Brale indenter.[16] The model is shown in Fig. 1.

In order to verify the results, three different mesh sizes were used. This is to reduce the mesh size effect. The TBC specimen models consist of four layers, TBC, a thermally grown oxide (TGO) layer, coating and substrate.

Four noded quadrilateral elements were used as part of the LSDYNA 970 finite element software package. The model is an axisymmetric solid and consists of 74 128 elements. The TBC system has 20 rows of element, whereas the coating layer has 10 rows of elements in the y direction. The TGO layer, which is extremely thin relative to the substrate layer, consists of one row of elements through the thickness. A fine finite grid was used to model the region below the indenter. Most elements involved in the contact region are very small, in the range 3–5 μm. The finite element model is shown in Fig. 2. A linux cluster super computer IBM x330 series was used to run the simulations.

In the coating layer, the elements are individual. They are constrained to each other with a plastic failure criterion. The adjacent nodes between the substrate and coating are also tied to each other with constrained plastic failure criterion. Plastic strain at which failure occurs for an N5 substrate is assumed to be the strain at

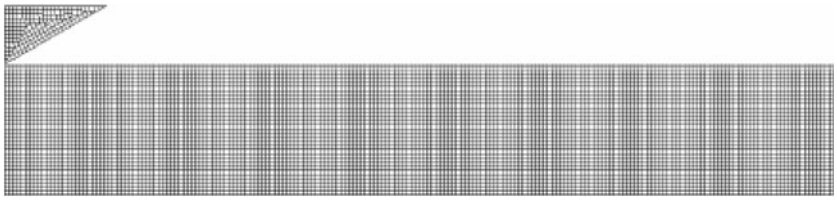

2 Finite element model

the yield point, since it is a very brittle material. This strain value is calculated from Table 1 as 0·0056.

Material

In the model, the substrate material is modelled using the Johnson and Cook material model.[17] The thermal and strain rate modelling capability of the Johnson–Cook material model are necessary in the present study because of the dynamic loading of the indenter and indentation at elevated temperature.

Johnson and Cook express the flow stress as

$$\sigma_y = (A + B\bar{\varepsilon}^{*p})(1 + c \ln \dot{\varepsilon}^*)(1 - T^{*m}) \quad (1)$$

where A, B, c, n and m are user defined constants, and $\bar{\varepsilon}^p$ is the effective plastic strain

$$\dot{\varepsilon}^* = \frac{\dot{\bar{\varepsilon}}}{\dot{\varepsilon}_0} = \text{effective plastic strain rate for } \dot{\varepsilon}_0 = 1\, s^{-1} \quad (2)$$

$$T^* = \frac{T - T_{room}}{T_{melt} - T_{room}} \quad (3)$$

Owing to nonlinearity in the dependence of flow stress on plastic strain, an accurate value of the flow stress requires iteration for the increment in plastic strain. However, using a Taylor series expansion with linearisation of the zone time, one can solve for σ_y with sufficient accuracy without iteration.

The strain at fracture is given by

$$\varepsilon^f = [D_1 + D_2 \exp D_3\sigma^*][1 + D_4 \ln \varepsilon^*][1 + D_5 T^*] \quad (4)$$

where $D_1,\ldots, D_5$ are input constants, and σ^* is the ratio of pressure divided by effective stress

$$\sigma^* = \frac{p}{\sigma_{eff}} \quad (5)$$

Fracture occurs when the damage parameter

$$D = \sum \frac{\Delta\bar{\varepsilon}^p}{\varepsilon^f} \quad (6)$$

This material model is applicable to the high rate deformation of many materials, including many metals. The Johnson–Cook model remains valid down to lower strain rates and even into the quasistatic regime. Therefore, although the Johnson–Cook material model is mainly good for explosive metal forming, ballistic penetration and impact, it can be used for indentation simulation at different strain rates. The constants $D_1,\ldots, D_5$ are obtained from literature.[18,19]

The bond coat in the TBC systems studied is a NiAl diffusion coating. The coating is electroplated onto the N5 substrate. The properties of the substrate and coating are given in Table 1. Using different substrates, the success of the method and coating materials, although they are not used for TBC systems, can be evaluated. The properties of these materials also are given in Table 1.

Table 2 Normalised delaminating radii *R/a* and calculated *Kc*[5]

Exposure time, h	*R/a*	K_c, MPa m^{-1}
10	7·6	0·83–2·09

Toughness calculation

In the literature, the toughness calculation of interfaces between SiC coatings and substrates of Si are shown in detail,[20] and the mechanism of adhesion between aluminium and aluminium oxide coating is also known.[21] In addition, numerical calculation values are available for the N5 NiAl TBC system. In order to compare the results, the same material properties were used in the present study. Stress–strain curves were also obtained from Vasinonta and Beuth.[5] The experimental values of the crack radius and corresponding interfacial energies calculated from models were also reported.[5] These values for the material studied are given in Table 2. The K_c value given in Table 2 is the experimental value. The same materials are used in the TBC system, therefore the same K_c value is used in the present study.

In the present study, the calculated values of interfacial toughness energies are compared with these values. This is the first constraint of the study. A 15 kg load was applied to the indenter.

In order to obtain interfacial toughness from a numerical model, as studied by Drory and Hutchinson, the total radial strain ε_r and circumferential strains ε_θ can be calculated by combining the residual strain ε_o with the strains caused by the indentation (calculated from the model). The relations are

$$\varepsilon_\theta = \varepsilon_\theta + \varepsilon_o \quad (7)$$

and

$$\varepsilon_r = \varepsilon_r + \varepsilon_o \quad (8)$$

where

$$\varepsilon_\theta = U^I \quad (9)$$

and

$$\varepsilon_r^I = \int \dot{\varepsilon}_r dt = \int \frac{V}{\Delta h} dt \quad (10)$$

Table 1 Material properties of coating and substrate

Material	Young's modulus, GPa	Poisson's ratio	Yield strength, MPa	Strain hardening exponent
Diamond (indenter)	1143·0	0·250	(Rigid)	No hardening
Hard substrate and coating				
NiAl (coating)	189·3	0·313	480–900	0·34
N5 (substrate)	137·9	0·380	775·6	0·44
Soft substrate and hard coating				
1040 steel (substrate)	210·0	0·29	160	0·20
Al_2O_3 (coating)				
Soft substrate and hard coating				
1040 steel (substrate)	210·0	0·29	160	0·20
Cr_2O_3 (coating)				

where V is velocity of indenter, and h is the depth of the indentation.

Equation (10) shows the velocity dependency of the radial strain. In the present study, no prestress is used so

$$\varepsilon_\theta = \varepsilon_\theta^{\mathrm{I}} \tag{11}$$

and

$$\varepsilon_{\mathrm{r}} = \varepsilon_{\mathrm{r}}^{\mathrm{I}} = \int \dot{\varepsilon}_{\mathrm{r}} \mathrm{d}t = \int \frac{V}{\Delta h} \mathrm{d}t \tag{12}$$

The residual strain is directly added to the calculations. Drory and Hutchinson[13] have advised modelling residual stresses by means of temperature constraints. Corresponding temperatures for known residual stresses are calculated and then applied as constraints on the coating layer.

Substituting ε_{r} and ε_θ as a function of R/a into the relation

$$\frac{2G(1-\nu)(1+\nu)}{Et} = \left[\varepsilon_{\mathrm{r}} \left(\frac{R}{a}\right) + \nu\varepsilon_{\mathrm{o}} \left(\frac{R}{a}\right)\right]^2 \tag{13}$$

and

$$\frac{2G(1-\nu)(1+\nu)}{Et} = \left[\varepsilon_{\mathrm{r}} \left(\frac{R}{a}\right) + \nu\varepsilon_{\mathrm{o}} \left(\frac{R}{a}\right) - \frac{(1-\nu^2)\varepsilon_\theta \left(\frac{R}{a}\right) - \left(\frac{R_1}{R}\right)^2}{(1-\nu)+(1+\nu)\left(\frac{R_1}{R}\right)^2}\right] \tag{14}$$

the distribution of energy release rate G for two extreme delamination process models, namely, (i) delamination leaving behind a very narrow annular plate of film, and (ii) delamination with an unbuckled annular plate of film left behind the crack tip, can be obtained. Because it typically involves buckling of the TBC, the distribution of the energy release rate G from the TBC indentation should lie between these two distribution curves.

Finally, the distribution of K versus R/a for both delamination models can be calculated by

$$K = \sqrt{G\bar{E}} \tag{15}$$

where

$$\bar{E} = \frac{E}{(1-\nu^2)} \tag{16}$$

This is the calculation method proposed by Drory and Hutchinson.[13]

The meanings of R and a are shown in Fig. 3.

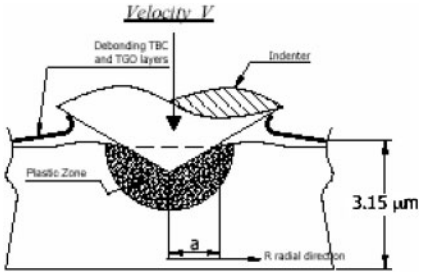

3 Indentation test

Results

Results of experiments

A modified hardness tester was used for the simple indentation method. In this apparatus, the indenter is sliding in a tube. The indenter has 500 g mass. The nose angle of the indenter is 120°. The drop height of the indenter is adjustable to any height. Increasing the drop height means increasing the velocity of the indenter. This apparatus is used for interfacial toughness measurements, and Table 3 shows the results for the three different TBC systems shown in Table 1.

These results are used for the corresponding plastic strain calculation in the finite element model. In other words, for the same crack radius for a given velocity, the plastic strain is sought.

These results are used for the corresponding plastic strain calculation in the finite element model. In other words, the plastic strain needs to be identified for the same crack radius for a given velocity.

Results of the model

In addition to the damage model used for the substrate material, the constrained node for failure has been defined between the coating and the substrate nodes. Even in the coating layer between each coating element, there are constrained nodes with plastic failure. This modelling technique is a good approach to seeing the circular crack radius. Figure 4 shows the radial displacement normalised with a distribution around the indentation zone. By means of this model, it was possible to generate values for the energy release rate for an axisymmetrically extending coating debondment. The radial displacement resulting from indentation as a function of the radial distance can therefore be identified. In order to study how the properties of the bond coat layer influence the results for radial surface

Table 3 Experimental results

TBC system	Drop height, mm	Indentation depth, mm	Corresponding velocity of indenter, m s^{-1}	Radius of circular crack measured, mm
NiAl (coating)/N5 (substrate)	50	0·44	0·49	3·43
	100	0·59	0·70	4·58
	200	0·83	0·99	6·48
	300	1·44	1·21	11·23
1040 steel (substrate)/Al_2O_3 (coating)	50	0·39	0·49	3·08
	100	0·53	0·70	4·11
	200	0·74	0·99	5·80
	300	1·29	1·21	10·08
1040 steel (substrate)/Cr_2O_3 (coating)	50	0·38	0·49	2·97
	100	0·51	0·70	3·96
	200	0·72	0·99	5·60
	300	1·24	1·21	9·70

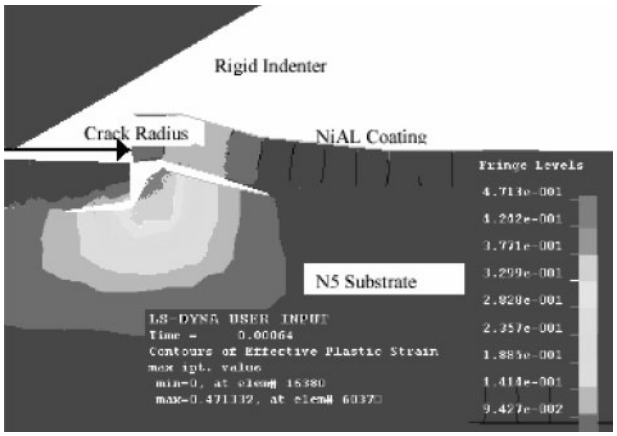

4 *U/a* versus *R/a*

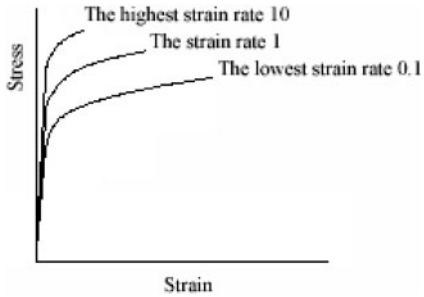

5 Strain rate dependent material behaviour

displacement, the results from the simulations of TBC model specimens are presented in Fig. 4. This model consists of two layers. The circular crack can be seen in Fig. 4.

As shown in Fig. 5, the higher velocities show lower displacements, whereas displacement values are the highest for the smallest velocity.

In Fig. 5, general strain rate dependent material behaviour is given in the tension. For the indentation test, the effect of strain rate on compression must also be investigated. It can be seen that, at higher strain rates, the stress–strain curve is shifted upwards. When the velocity of deformation is increased, the material behaves as if it is harder.

The effect of this behaviour on the bending geometry is given in Fig. 6. The radial displacement U for increasing strain rate increases from A to C. The higher the strain rates, the higher the displacement. The reason for this is that material loses its bending flexibility as the

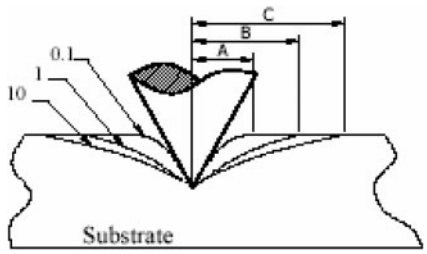

6 Effect of strain rate on radial displacement *U*

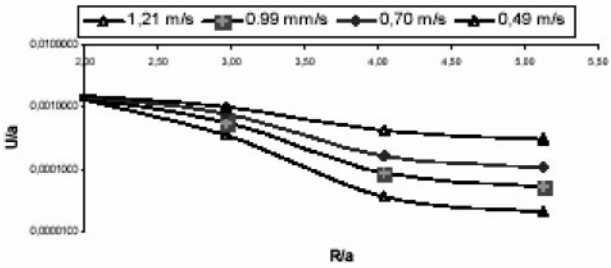

7 Effects of different velocities on the radial displacement (*U/a*) for N5–NiAl system

strain rate increases. Therefore, although the indentation depth becomes constant, the radial displacement increases.

This explains why high velocity deformation near the impact produces a circular crack, whereas static loading for the same amount of mass does not produce a crack. The circular crack radius measured from experiments is $\sim 5a$. This value is used to find the plastic strain at the interface between the coating and the substrate.

In Fig. 7, the effects of velocity on the radial displacement U normalised by a are given. Increasing velocity decreases the U/a ratio. The higher the velocity, the lower the U/a ratio.

The stresses which occur owing to these deformations in the radial and transverse directions are obtained from simulations which were also normalised with residual stress values and plotted again with respect to R/a values. The residual stress values are 70 MPa for the compressive stress and 20 MPa for the tensile stress. Figure 8 shows the relationship obtained between σ_r/σ_o+1 (radial stress normalised with residual stress) with respect to the R/a value for different deformation velocities. In the same figure, σ_t/σ_o+1 (tangential stress normalised with residual stress) values are also plotted.

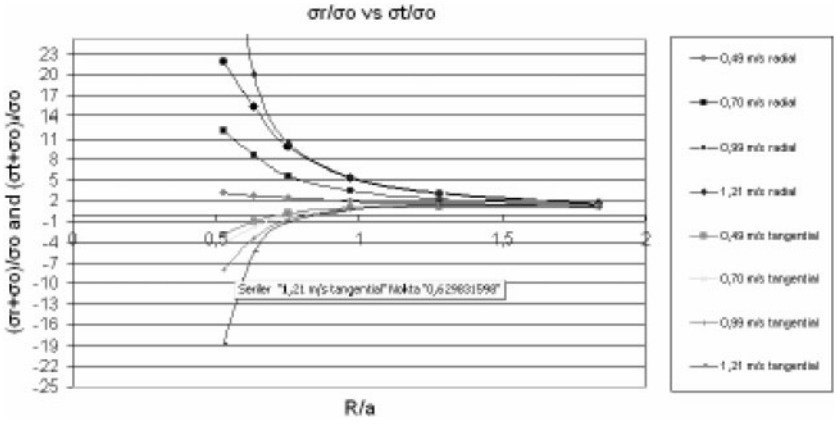

8 Effect of different velocities on radial and transverse stresses for N5–NiAl system

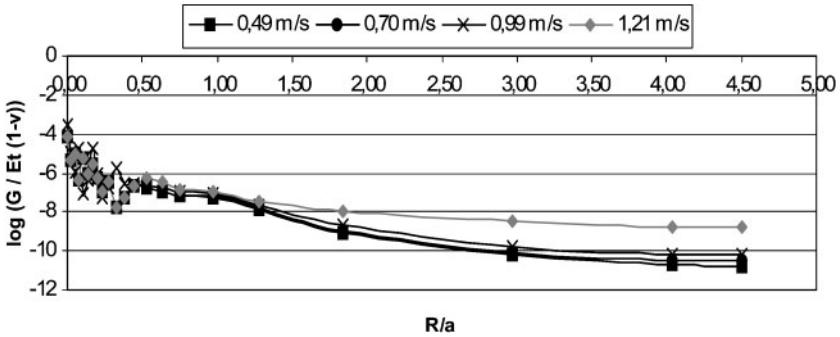

9 Normalised energy release rate as function of compressive residual film strain and distance from indentation for N5–NiAl system

Figure 8 summarises the results for three different major loads. The plot shows that the bond coat layer affects the results only when R/a is small. When $R/a>3$, the results from the N5 only model are close to the results from the bond coat/N5 model. Moreover, the plot also shows that, in the range $2<R/a<5$, the indent load level is not significant to the distribution of U.

Several observations can be made comparing the distribution of the radial displacement in each case. First, for the TBC specimen sized model, ther indent load affects the results when R/a is higher than $\sim$5, and the plots show that larger applied loads produce larger displacements. To see the effect of substrate size, results from a model using identical conditions as the TBC specimen model except that the model size is changed to the large substrate size. By comparing the results from the standard size and large TBC model, it is clear that the size of the specimen seriously affects the results. The radial displacement from both a standard and large size TBC model agree well at small R/a but, when $R/a>5$, the displacement from the standard size model decreases at a much slower rate than for the large size model. The reason is that for $R/a>5$, the radial displacements from the standard size model begin to experience the free effect from the edge of the specimen, which allows material to move freely outwards in the radial direction. In contrast, in the large size model, the material cannot move freely because it is resisted by the surrounding substrate.

The procedure for extracting interfacial toughness from the numerical indentation model and the radius of delamination observed in an indent test has been outlined by Drory and Hutchinson.[13] First, the total strain and circumferential strains can be calculated by combining the residual strain with the strains caused by the indentation. The interfacial toughness of the material is then calculated using equations (7)–(16).

Figure 9 shows the normalised energy release rate that is necessary for the calculation of toughness. In the figure, the effect of deformation velocities on the energy release rate are shown. The effect is clear at locations far away from the indentation zone. Figure 10 shows how these deformation velocities affect the K_c value. At a high velocity, the coating and substrate behave as if the interfacial toughness is increased. Although interfacial toughness is a material property, it is also a function of temperature and strain rate.

Conclusions

In order to remove the restrictions in the application of the indentation test to calculate interfacial toughness energy, a new approach is tested in the present study. Instead of using a static loading of 15 kg, the load is applied with a constant velocity. This dynamic loading supported the formation of a circular crack and therefore the use of this simple method even for ductile substrates. These impact loading results therefore encourage the finite element modelling of the indent test for dynamic loading. In the model, the constrained tied break nodes were employed to predict the radius of the crack. For these constrained nodes, the plastic strain failure value for the coating is found for the same circular crack radius as that obtained from experiments. In conclusion, the use of dynamic loading can lead to an

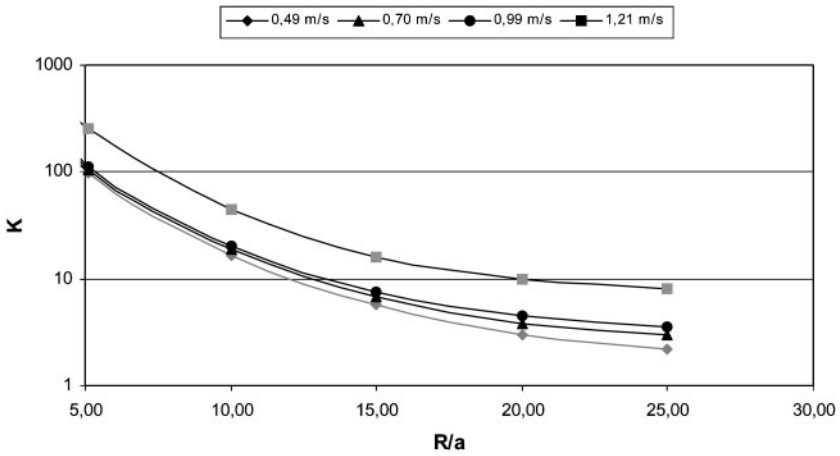

10 Change in interfacial toughness for different deformation velocities for N5–NiAl system

increase in the application range of the indentation method for interfacial toughness measurement.

Acknowledgements

The author would like to thank Dr Mehmet Yeginmen and BYM Firm for their support in the use of the supercomputer and LS-Dyna software, and also Mr Cevat Sarioglu for his invaluable encouragement to study in this field.

References

1. G. Cianflone, F. M. Furgiuele and G. Sciume: *Eng. Fract. Mech.*, 2004, **71**, 669–679.
2. U. Schulz, M. Peters, Fr.-W. Bach and G. Tegeder: *Mater. Sci. Eng.* A, 2003,**362**,61–80.
3. S. B. Sinnott and E. C. Dickey: *Mater. Sci. Eng. R*, 2003, **43**, 1–59.
4. A. G. Evans, D. R. Mumma, J. W. Hutchinson, G. H. Meier and F. S. Pettit: *Progr. Mater. Sci.*, 2001, **46**, 505–553.
5. A. Vasinonta and J. L. Beuth: *Eng. Fract. Mech.*, 2001, **68**, 843–860.
6. R. M. Souza, G. G. W. Mustoe and J. J. Moore: *Thin Solid Films*, 2001, **392**, 65–74.
7. A. Abdul-Baqi and E. Van der Giessen: *Thin Solid Films*, 2001, **381**, 143–154.
8. B. Ekici: *J. Surf. Eng.*, 2004, **20**, 37–42.
9. M. R. Begley, D. R. Mumm, A. G. Evans and J. W. Hutchinson: *Acta Mater.*, 2000, **48**, 3211–3220.
10. J. Mackerle: *Finite Elem. Anal. Des.*, 2000, **34**, 113–124.
11. G. Thurn, G. A. Schneiderb, H. -A. Bahr and F. Aldingera: *Surf. Coat. Technol.*, 2000, **123**, 147–158.
12. K. Zeng, E. Söderlund, A. E. Gıannakopoulos and D. J. Rowcliffe: *Acta Mater*., 1996, **44**, 1127–1141.
13. M. D. Drory, and J. W. Hutchinson: *Proc. R. Soc. (London) A*, 1996, **452**, 2319–2341.
14. S. Bose and D. M. Jeanine: Proc. 'Thermal barrier coating workshop', NASA Lewis Research Center, Cleveland, 27–29 March; 1995, Nasa Conference Publications 3312, 63–78.
15. C. Bartuli, L. Bertamini, S. Matera and S. Sturlese: *Mater. Sci. Eng. A*, 1995, **199**, 229–237.
16. A. E. Gıannakopoulos, P. L. Larsson and R. Vestergard: *Int. J. Solid Struct.*, 1994, **31**, 2679–2708.
17. G. R. Johnson and W. H. Cook: Proc. 7th Int. Symp. on 'Ballistics', The Hague, 1983.
18. G. R. Johnson and T. J. Holmquist: 'Test data and computational strength and fracture model constants for 23 materials subjected to large strains, high strain rates, and high temperatures', LA-11463-MS, Los Alamos National laboratory, 1989.
19. G. R. Johnson and W. H. Cook: *Eng. Fract. Mech.*, 1985, **21**, 31–48.
20. A. S. Argon, V. Gupta, H. S. Landis and J. A. Cornie: *J. Mater. Sci.*, 1989, **24**, 1207–1218.
21. K. L. Luthra and C. L. Briant: *Oxid. Met.*, 1986, **26**, 397–416.